JACS
JOURNAL OF THE AMERICAN CHEMICAL SOCIETY
Article
pubs.acs.org/JACS

Synthesis and Characterization of Carbazolide-Based Iridium PNP Pincer Complexes. Mechanistic and Computational Investigation of Alkene Hydrogenation: Evidence for an Ir(III)/Ir(V)/Ir(III) Catalytic Cycle

Chen Cheng,[†] Bong Gon Kim,[†,§] Damien Guironnet,[†] Maurice Brookhart,*[,†] Changjian Guan,[‡] David Y. Wang,[‡] Karsten Krogh-Jespersen,*[,‡] and Alan S. Goldman*[,‡]

[†]Department of Chemistry, The University of North Carolina at Chapel Hill, Chapel Hill, North Carolina 27599, United States
[‡]Department of Chemistry and Chemical Biology, Rutgers, The State University of New Jersey, New Brunswick, New Jersey 08903, United States

Supporting Information

ABSTRACT: New carbazolide-based iridium pincer complexes (^{carb}PNP)Ir(C_2H_4), **3a**, and (^{carb}PNP)Ir(H)$_2$, **3b**, have been prepared and characterized. The dihydride, **3b**, reacts with ethylene to yield the *cis*-dihydride ethylene complex *cis*-(^{carb}PNP)Ir(C_2H_4)(H)$_2$. Under ethylene this complex reacts slowly at 70 °C to yield ethane and the ethylene complex, **3a**. Kinetic analysis establishes that the reaction rate is dependent on ethylene concentration and labeling studies show reversible migratory insertion to form an ethyl hydride complex prior to formation of **3a**. Exposure of *cis*-(^{carb}PNP)Ir(C_2H_4)(H)$_2$ to hydrogen results in very rapid formation of ethane and dihydride, **3b**. DFT analysis suggests that ethane elimination from the ethyl hydride complex is assisted by ethylene through formation of (^{carb}PNP)Ir(H)(Et)(C_2H_4) and by H_2 through formation of (^{carb}PNP)Ir(H)(Et)(H_2). Elimination of ethane from Ir(III) complex (^{carb}PNP)Ir(H)(Et)(H_2) is calculated to proceed through an Ir(V) complex (^{carb}PNP)Ir(H)$_3$(Et) which reductively eliminates ethane with a very low barrier to return to the Ir(III) dihydride, **3b**. Under catalytic hydrogenation conditions (C_2H_4/H_2), *cis*-(^{carb}PNP)Ir(C_2H_4)(H)$_2$ is the catalyst resting state, and the catalysis proceeds via an Ir(III)/Ir(V)/Ir(III) cycle. This is in sharp contrast to isoelectronic (PCP)Ir systems in which hydrogenation proceeds through an Ir(III)/Ir(I)/Ir(III) cycle. The basis for this remarkable difference is discussed.

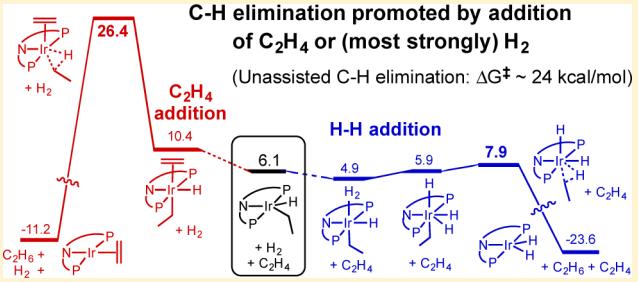

1. INTRODUCTION

Dehydrogenation of alkanes to alkenes using homogeneous catalysts has received intense interest in recent years.[1−4] Dehydrogenation reactions can be run in an "acceptorless" mode,[5] but most commonly the reaction is run as a transfer dehydrogenation where a sacrificial alkene is used as a hydrogen acceptor. Transfer dehydrogenation is one of the two key reactions in the dual catalytic system used to achieve alkane metathesis, a potentially important reaction for converting low molecular weight hydrocarbons to higher molecular weight hydrocarbons useful as fuels.[6−8] Conversion of linear alkanes to aromatics under homogeneous conditions has also been achieved via multiple transfer dehydrogenations coupled with electrocyclic ring closure of intermediate trienes.[9]

While a number of early reported systems based on late transition-metal complexes showed promise,[10] a major breakthrough was the discovery by Kaska and Jensen that the iridium pincer complex [C_6H_3-2,6-($CH_2P(t$-Bu)$_2$)$_2$]IrH_2, (^{tBu}PCP)IrH_2, catalyzes the transfer dehydrogenation reaction between cyclooctane (COA) and *t*-butylethylene (TBE) to form cyclooctene (COE) and *t*-butylethane (TBA) with high turnover numbers at 200 °C (eq 1);[11] this reaction is often regarded as a benchmark for screening catalysts for transfer dehydrogenation.

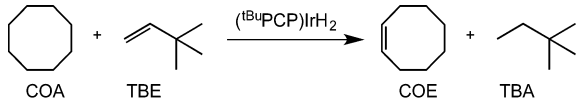

(1)

Following this initial report, extensive investigations of transfer dehydrogenations using the (^{tBu}PCP)IrH_2 pincer complex and many other PCP-type derivatives have been reported.[12−17] The three most thoroughly examined frameworks, "PCP", "POCOP",[18,19] and "PCOP",[7] are shown in Figure 1. Extensive screening reactions, mechanistic studies, and DFT investigations of these systems have been reported.[14,19−24]

Received: February 14, 2014
Published: April 18, 2014

   dx.doi.org/10.1021/ja501572g | J. Am. Chem. Soc. 2014, 136, 6672−6683

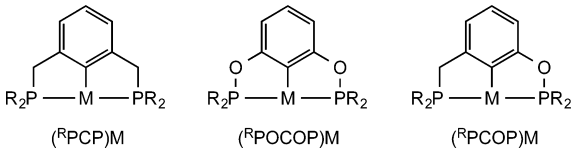

Figure 1. Common PCP-type pincer complexes.

The basic mechanism established for transfer dehydrogenation using the COA/TBE system is shown in Scheme 1. In the case of the ($^{t\mathrm{Bu}}$PCP)Ir system, at low TBE concentration the catalyst resting state is the dihydride and the turnover-limiting step is hydrogenation of TBE, while at high TBE concentration the resting state is the vinyl hydride and dehydrogenation is turnover limiting.[22] For the ($^{t\mathrm{Bu}}$POCOP)Ir system, the resting state is the alkene complex, and dehydrogenation is turnover limiting.[19]

Scheme 1. Hydrogen Transfer Between COA and TBE using PCP- and POCOP-Iridium Pincer Complexes

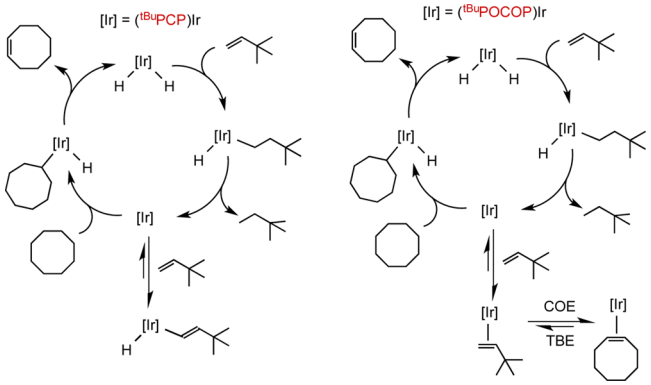

Convenient rates for transfer dehydrogenation for the PCP and POCOP systems occur at temperatures in the range of ca. 125−200 °C. Thus, temperatures employed for alkane metathesis using these catalysts must also be in this range despite the fact that the molecular olefin metathesis cocatalysts often decompose rapidly at these temperatures and operate more effectively at lower temperatures.[25] In part for this reason it is desirable to develop new transfer dehydrogenation catalysts that function at lower temperatures.

DFT calculations have shown that the thermodynamic favorability of oxidative addition of nonpolar substrates, including H_2 and RH, to the fragment XML_2 (M = Ir, Rh) increases as the σ-donating ability of X decreases.[26] The direction of this effect is opposite that which is generally accepted for oxidative addition, and moreover, the magnitude is surprisingly large. For example, addition of CH_3−H to $Ir(PH_3)_2F$ is calculated to be far more exothermic (ΔH = −34.9 kcal/mol) than addition to the much more electron-rich metal center of $Ir(PH_3)_2CH_3$ (ΔH = −9.3 kcal/mol). In view of these results we felt it would be of interest, in the context of transfer dehydrogenation, to examine analogues of (PCP)Ir and (POCOP)Ir in which the central iridium-coordinated sp^2 carbon is replaced by a less σ-donating sp^2 nitrogen group. Toward this end, ligand **1**, bearing a carbazolide backbone, was targeted for synthesis along with the iridium complexes **3a**,**b** (Figure 2). These ligands bear a close relationship to the Ozerov PNP ligand;[27] however, based on the pK_a values of the neutral ligands,[28] the central nitrogen atom in **3a**,**b** is expected to be a weaker σ donor than in the Ozerov complexes **2a**,**b**.

This manuscript reports the synthesis and characterization of the carbazolide ligand **1** and iridium complexes **3a**,**b**. In preliminary screening using the COA/TBE system, the iridium carbazolide system exhibited quite low transfer dehydrogenation activity at 200 °C without apparent decomposition. Since alkene hydrogenation is a critical part of the transfer cycle, we then probed these systems for simple alkene hydrogenation. These studies have revealed unusual features of these reactions; especially noteworthy is the observation that H_2 can play a critical role by facilitating reductive elimination of alkane from the metal center.

2. RESULTS

2.1. Synthesis of Carbazole-Based Ligands and Iridium Complexes. The carbazolide ligand **1′** was prepared as described in Scheme 2. The 1,8-dibromide precursor **6** was prepared as previously described.[29] Since the bromination is selective for the 3,6-positions on the carbazole ring, these positions were protected with methyl groups; subsequent bromination occurs at the 1,8-positions to yield **6**. Carboxylation of **6** gave diacid **7**, and reduction of **7** with $LiAlH_4$ to the diol **8** and bromination using PBr_3 afforded the dibromide **9**. Nucleophilic substitution using HP(*i*-Pr)$_2$ gave the ^{carb}PNP ligand **1**. Deprotonation of **1** with LiN(TMS)$_2$ yields a lithium complex, **1′**, which is not stable in solution and must be used immediately. Reaction of the *in situ* generated lithium salt **1′** with $[(C_2H_4)_2IrCl]_2$ followed by filtration and removal of solvent and HN(TMS)$_2$ under vacuum gave the Ir(I) ethylene complex **3a** as a brown solid in 78% yield.

2.2. Screening 3a for Transfer Dehydrogenation. The newly prepared complex **3a** was screened for the benchmark reaction of hydrogen transfer between COA and TBE. Using the same conditions as previously reported for the ($^{t\mathrm{Bu}}$POCOP)Ir system (0.03 mol % of **3a** and a 1:1 molar ratio of COA:TBE)[14] at 200 °C gave traces of cyclooctene but overall poor activity. Monitoring by NMR spectroscopy shows no catalyst decomposition or catalyst deactivation (e.g., formation of a binuclear dimer).[16] Rather, surprisingly, under these conditions of high TBE concentration the resting state of the carbazole-based iridium complex **3** was shown to be the dihydride species **3b**, suggesting that hydrogenation is turnover limiting for

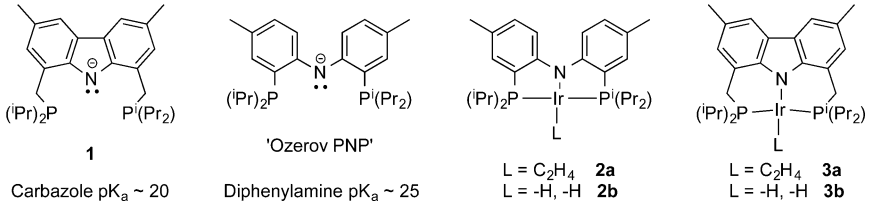

Figure 2. Comparison of carbazolide and Ozerov-type anionic PNP-type pincer ligands and their iridium complexes.

dx.doi.org/10.1021/ja501572g | J. Am. Chem. Soc. 2014, 136, 6672−6683

Scheme 2

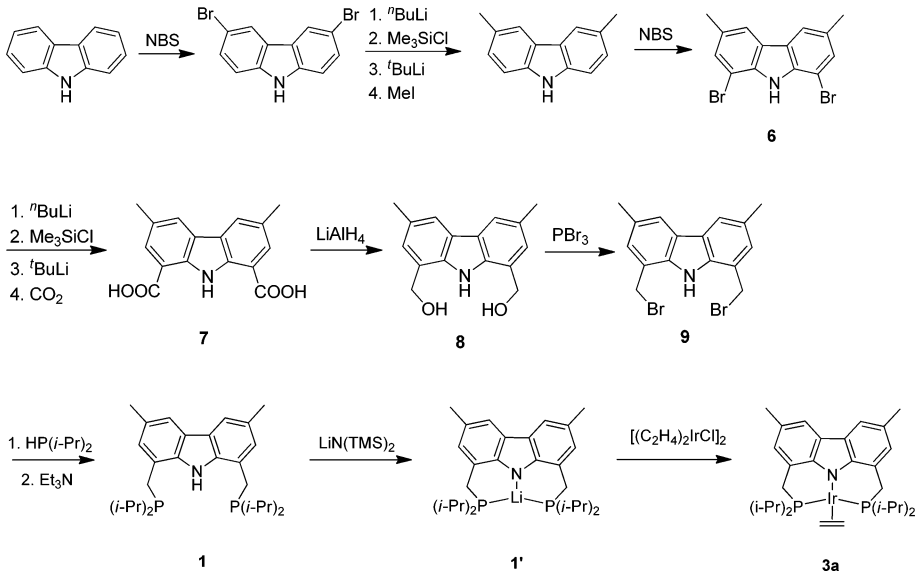

transfer dehydrogenation catalyzed by complex **3**. In light of these observations, we initiated a detailed study of the olefin hydrogenation reactions with the carbazolide system using the simplest olefin, ethylene. These investigations are described below.

2.3. Ethylene hydrogenation studies employing carbazolide complexes 3a and 3b. Purging hydrogen through a benzene solution of ethylene complex **3a** at room temperature (rt) resulted in the formation of the corresponding iridium(III) dihydride species **3b** within 10 min accompanied by the formation of 1 equiv C_2H_6 (eq 2). However, when C_2H_4

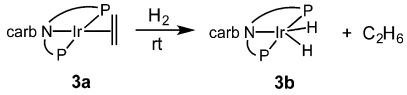

(2)

was purged through a solution of **3b** at rt in the absence of H_2, no hydrogenation was observed over 24 h (eq 3). Stoichiometric hydrogenation of C_2H_4 with **3b** under a C_2H_4 atmosphere (eq 4) proceeded at 70 °C with a half-life of ca. 40 min ($\Delta G^{\ddagger} \sim 26$ kcal/mol)

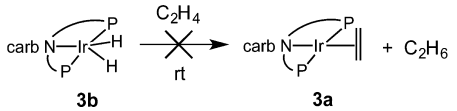

(3)

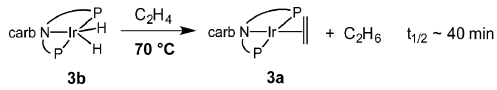

(4)

This behavior is in dramatic contrast to that of the ^{tBu}POCOP iridium(III) dihydride complex, which hydrogenates a much bulkier alkene, COE, at −70 °C.[19] (^{tBu}PCP)IrH_2 also reacts with the bulky TBE to give TBA under relatively mild conditions (ca. 55 °C) and with 1-alkenes rapidly even at subambient temperatures.[22,30]

A closer look at the reaction of iridium dihydride **3b** with C_2H_4 at −50 °C revealed the immediate and complete conversion to an Ir(III) ethylene dihydride species, **3c**, under excess C_2H_4 (eq 5). The *cis*-dihydride geometry is indicated by

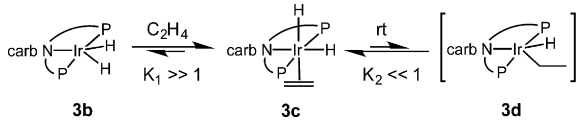

(5)

the appearance of two nonequivalent hydride resonances, with the hydride *trans* to the anionic nitrogen at a lower chemical shift (−11.83 ppm, dt, $J_{H,H}$ = 5.2 Hz, $J_{H,P}$ = 18.2 Hz) and the hydride *trans* to C_2H_4 at a higher chemical shift (−23.99 ppm, dt, $J_{H,H}$ = 5.8 Hz, $J_{H,P}$ = 13.6 Hz).[31]

Binding of C_2H_4 to iridium dihydride **3b** to form iridium ethylene dihydride **3c** is reversible and thermodynamically favored ($K_1 \gg 1$, eq 5). The free energy barrier for exchange of free C_2H_4 with **3c** at −20 °C was estimated to be ∼13 kcal/mol based on NMR line broadening of both the bound C_2H_4 and Ir−H signals. A large positive $\Delta S^{\ddagger}$ value (40 ± 12 cal·K^{-1}·mol^{-1}) was determined for the exchange, and the rate of exchange was found to be independent of the C_2H_4 concentration, which is consistent with a dissociative mechanism for C_2H_4 exchange. At rt, the rate of C_2H_4 dissociation is fast on the NMR time scale, and the hydride resonances are not observable as they are broadened into the baseline.

Although ethylene dihydride complex **3c** is the resting state under C_2H_4 at rt, it remained to be determined whether ethylene insertion into an Ir−H bond or reductive elimination of ethane from the resulting iridium ethyl hydride is rate-determining for C_2H_4 hydrogenation. When C_2H_4 was purged through a solution of deuterium-labeled **3c**-d_2 at rt, protio-**3c** formed (eq 6). The exchange of hydrogen for deuterium

(6)

indicates that **3c** is in equilibrium with the insertion product, the ethyl hydride complex **3d**, with $K_2 \ll 1$ since **3d** was not observed experimentally (eq 7). This reversible insertion of C_2H_4 at rt strongly suggests that the rate-limiting step for

dx.doi.org/10.1021/ja501572g | J. Am. Chem. Soc. 2014, 136, 6672−6683

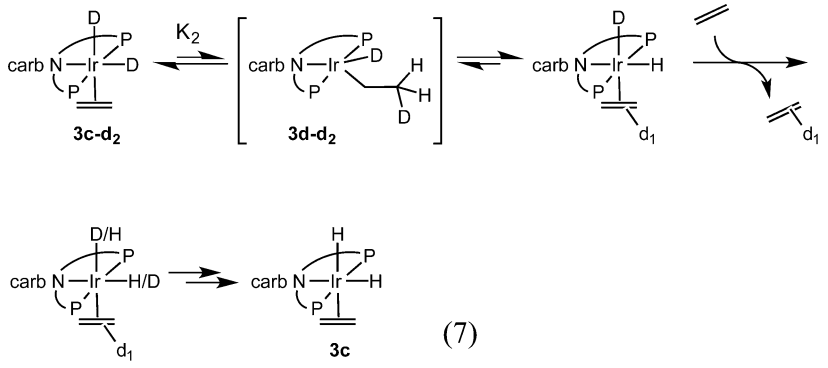

Scheme 3. Proposed Pathways (Unimolecular and Bimolecular) For the Reaction of 3c with C_2H_4 To Yield 3a and C_2H_6[a]

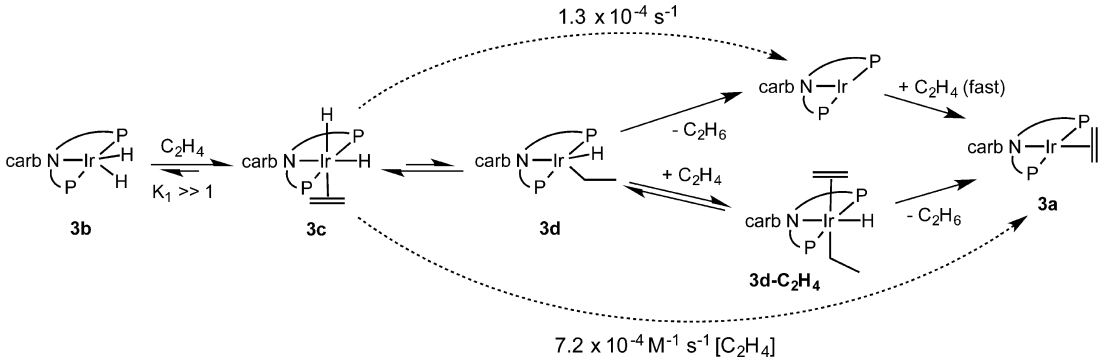

[a]Rate constants determined at 75 °C.

hydrogenation of C_2H_4 with **3b** under excess C_2H_4 is reductive elimination of C_2H_6. The rate of H/D scrambling obtained using C_2D_4 indicates a barrier to insertion of $\Delta H^{\ddagger}$ = 21.5 ± 0.8 kcal/mol at −10 °C, with a small $\Delta S^{\ddagger}$ value of 3.3 ± 2.8 eu, consistent with an intramolecular rearrangement reaction.

Details of the reductive elimination of ethane from iridium ethyl hydride **3d** were investigated. Kinetic experiments revealed that the rate of stoichiometric hydrogenation of C_2H_4 with dihydride **3b** under excess C_2H_4 (eq 4) is dependent on $[C_2H_4]$ in the range 0.05−0.9 M at 75 °C according to eq 8.

$$k_{obs} = 1.3 \pm 0.13 \times 10^{-4}\ s^{-1} + 7.2 \pm 0.28 \times 10^{-4}\ M^{-1}\ s^{-1}[C_2H_4] \quad (8)$$

The nonzero value of k_{obs} in the limit as $[C_2H_4]$ approaches zero is consistent with a unimolecular pathway that proceeds via elimination of ethane from **3d**. The $[C_2H_4]$-dependent term suggests that the major pathway under high C_2H_4 pressure involves, in addition to the ethylene molecule that rapidly coordinates to give **3c**, a second molecule of ethylene in the transition state (TS) for reductive elimination of ethane from **3d**; this would be consistent with formation of the six-coordinate species (^{carb}PNP)Ir(H)(C_2H_5)(C_2H_4) (**3d-C_2H_4**) prior to ethane elimination (Scheme 3).

In the reaction of ethylene complex **3a** with H_2 to form dihydride **3b** and ethane (eq 2), low-temperature NMR experiments revealed the quantitative formation of ethylene dihydride **3c** prior to production of any **3b** and ethane. The half-life for conversion of **3c** to ethane and dihydride **3b** under 1 atm H_2 is ca. 5 min at 25 °C, which is much faster than the conversion of **3c** to ethane and ethylene complex **3a** under ethylene. (In fact, this rate of reaction of **3c** under H_2, to give **3b** and ethane, is only marginally slower than the rate of migratory insertion of **3c** indicated by the H/D exchange experiments.)

These observations suggest that the ethyl hydride complex **3d**, formed by migratory insertion of **3c**, is trapped by H_2 to form a six-coordinate dihydrogen complex, **3d-H_2**, and that this complex undergoes elimination of ethane at a rate much greater than ethane elimination from the five-coordinate **3d** (eq 9).

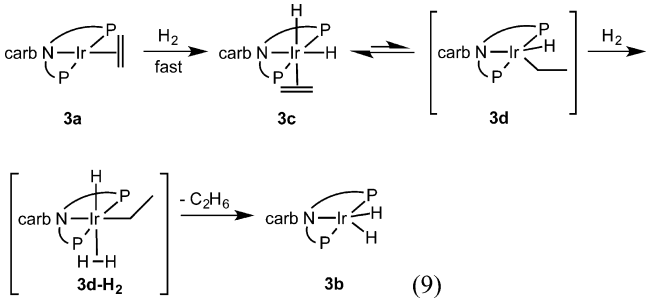

The dihydrogen complex **3d-H_2** is not spectroscopically detectable under 1 atm H_2 and, since the rates of migratory insertion of **3c** and overall hydrogenation under 1 atm H_2 are similar, this indicates that the barrier for release of ethane from **3d-H_2** is significantly less than 21 kcal/mol (DFT studies discussed below support this view and provide additional mechanistic details).

Acceleration by H_2 of propene and TBE hydrogenation by the carbazole-based dihydride **3b** was also observed. In the absence of excess H_2, no reaction of propene or TBE with **3b** was observed even at 100 °C (eq 10). However, when a mixture of propene/H_2 or TBE/H_2 was introduced to **3b**, rapid catalytic hydrogenation of olefin was observed at rt (eq 11). The catalyst resting state in each of these hydrogenations is the dihydride complex **3b**. These observations further support the contention that alkane elimination from the iridium center in

dx.doi.org/10.1021/ja501572g | J. Am. Chem. Soc. 2014, 136, 6672−6683

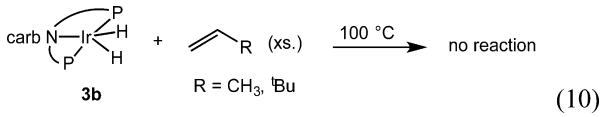

(10)

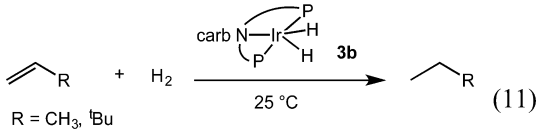

(11)

the carbazolide system is facilitated by H_2. The overall catalytic cycle is shown in Figure 3. Although we could not observe

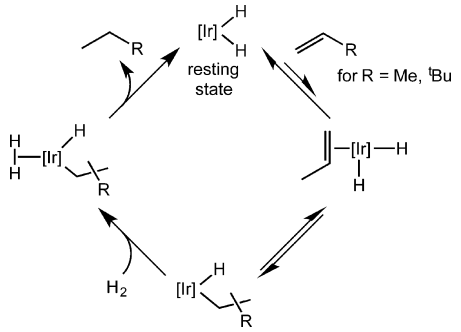

Figure 3. Proposed catalytic cycle for hydrogenation of propene and TBE with **3b**.

stable alkene dihydride complexes (analogous to the ethylene dihydride complex **3c**) in the reactions of **3b** with excess propene or TBE, deuterium incorporation into the hydride positions was observed when propene-d_6 was purged through a solution of dihydride **3b** at rt, showing that reversible insertion of propene takes place even at rt (eq 12).

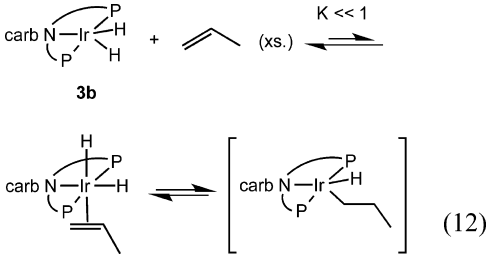

(12)

2.4. DFT Studies of the Hydrogenation of Alkenes with Iridium Carbazole-Based Catalysts. The results of DFT calculations on the reactions of carbazolide iridium dihydride **3b** with ethylene and dihydrogen are consistent with and quite helpful in explaining the experimental observations. The calculations employed the recently developed M11 functionals[32] and valence basis sets of triple-ζ plus polarization quality; complete computational details are provided in the Experimental Section and in Supporting Information.

*2.4.1. Reaction of Dihydride **3b** with Ethylene to Afford Ethyl Hydride **3d**.* In accord with experiment, the reaction of **3b** with ethylene is calculated to yield the *cis*-dihydride ethylene complex **3c**. The addition is calculated to be exergonic, and the kinetic barrier is calculated to be quite low, $\Delta G^{\ddagger}$ = 5.0 kcal/mol, consistent with the immediate formation of **3c** observed upon addition of ethylene to a solution of **3b**. The calculated free energy of olefin addition, ΔG°_{calc} = −2.9 kcal/mol, is about at the upper limit consistent with experiment since the observed equilibrium lies fully to the right indicating that ΔG° < ca. −3 kcal/mol. The calculated barrier to dissociation, $\Delta G^{\ddagger}$ = 7.9 kcal/mol, is somewhat lower than the barrier of ca. 13 kcal/mol indicated by the experimentally determined rate of exchange with free ethylene. These results may suggest that ligand binding energies are understated by the computational method. It is worth noting, as we compare associative vs dissociative reaction pathways below, that this propensity would only lead to a computational bias in favor of dissociative pathways.

In contrast to the kinetically facile addition of ethylene to dihydride **3b** to give the *cis*-dihydride ethylene complex **3c** ($\Delta G^{\ddagger}$ = 5.0 kcal/mol), ethylene addition along a symmetrical pathway to give the *trans*-dihydride is calculated to have an extremely high kinetic barrier ($\Delta G^{\ddagger}$ > 40 kcal/mol) as well as somewhat unfavorable thermodynamics (ΔG°_{calc} = +9.1 kcal/mol).[33] In agreement with these calculated values, the *trans*-dihydride was never observed experimentally in the course of this work.

Locating a plausible TS for the seemingly simple insertion reaction of the coordinated ethylene of **3c** into the Ir−H bond turned out to be computationally intricate. The product of olefin insertion, ethyl hydride **3d**, is a pentacoordinate metal d^6 species and hence susceptible to pseudo-second-order Jahn−Teller effects; accordingly, several square-pyramidal (SQP) or trigonal-bipyramidal (TBP) structures may exist for **3d**.[34] The lowest energy conformer of **3d** is SQP with ethyl apical and the carbazolide nitrogen and hydride ligands oriented *trans* to each other (>N−Ir−H = 177.7°, see Scheme 4); this is a T_C

Scheme 4. Species 3c, TS-3c-3d, and 3d[a]

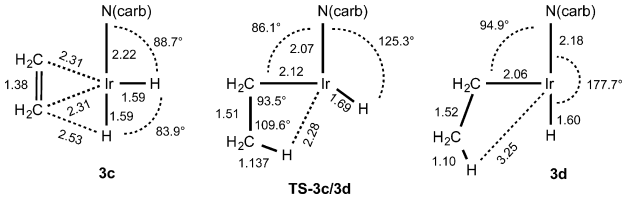

[a]Metrics are shown (bond lengths in Å) for the coordination sphere excluding the coordinating P atoms (i.e., for the ligands in the approximate plane bisecting the P−Ir−P axis).

structure in the notation of Eisenstein and Pelissier.[35] The T_C conformer of **3d** is 6.1 kcal/mol above **3c** in free energy; other SQP structures located, namely T_H and T_N, are found to be 9.7 and 35.5 kcal/mol above **3c**, respectively. A TBP structure, denoted Y_N (>H−Ir−C = 75.9°), is 8.1 kcal/mol above **3c.**

Some geometrical parameters pertaining to the lowest energy conformers of **3c**, **3d**, and the TS of lowest energy connecting them, **TS-3c/3d**, are shown in Scheme 4. In **TS-3c/3d** the C−H bond is nearly fully formed (d(C−H) = 1.137 Å), and the Ir−H distance (d(Ir−H) = 2.28 Å) remains well below the sum of the van der Waals radii of Ir and H (3.1 Å),[36] indicating the presence of an agostic interaction.[37] Examination of the reaction coordinate evaluated at **TS-3c/3d** shows predominantly a swinging motion of the hydride ligand, i.e., a substantial increase of the N−Ir−H angle when progressing toward **3d**, with a smaller component best described as loss of the apparent agostic interaction.

Disturbingly, the free energy of **TS-3c/3d** is calculated to be 32.8 kcal/mol above that of **3c**, while the experimental value, implied by the rate of H/D exchange observed for **3c**-d_2, is only 21 kcal/mol. Single point calculations (M11 optimized

dx.doi.org/10.1021/ja501572g | J. Am. Chem. Soc. 2014, 136, 6672−6683

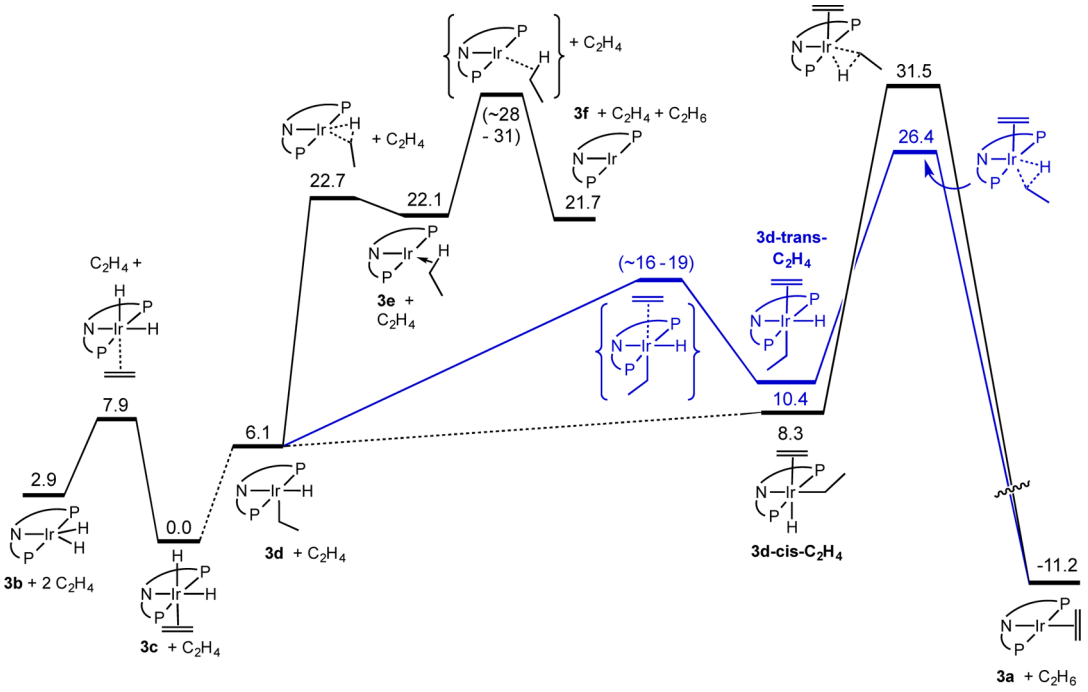

Figure 4. Calculated free energies (kcal/mol) for the hydrogenation of ethylene by **3b** under 1 atm ethylene at 25 °C (favored path in blue). Structures in brackets ({ }) are not calculated geometries; they are shown to illustrate the barriers estimated (see text) for steps that do not appear to proceed via a TS. Computational estimates for the energy of **TS-3c/3d** vary greatly (see text); hence, the barrier for ethylene insertion is not shown.

geometries) at the MP2 level predict an even higher barrier (44.0 kcal/mol), whereas CCSD calculations (with a smaller valence basis set) yield 30.8 kcal/mol. Other commonly used "Minnesota functionals" such as M11-L, M06-L, or M06 produced optimized ethylene insertion TS structures very similar to **TS-3c/3d**, but their free energies were only 23.6, 27.7, and 25.9 kcal/mol, respectively, above **3c**.[38] The overestimation of the barrier by single-determinant based methods may reflect that proper descriptions of the potential energy surfaces and electronic states of d^6 ML_5-type species require minimally the use of two-configuration wave functions.[39] **TS-3c/3d** has a narrow N−Ir−C angle of 86.1° and hence shows resemblance to a TBP Y_H-type structure. Whether a multiconfiguration approach would produce a TS structure and energy for olefin insertion significantly different from **TS-3c/3d** is, however, well outside the scope of the present work.[40]

*2.4.2. Reaction of Ethyl Hydride **3d** under an Ethylene Atmosphere. 2.4.2.1. The Unassisted (Dissociative) Pathway.* For the PCP-type (phenyl-based) pincer analogues of complex **3d**, calculations indicate that reductive elimination with loss of ethane is exergonic. For example, using the computational methods applied to the present (^{carb}PNP)Ir system we calculate that $\Delta G°$ for loss of ethane from (^{iPr}PCP)Ir(ethyl)(H) is −2.5 kcal/mol ($\Delta H°$ = +10.1 kcal/mol). In contrast, for loss of ethane from ^{carb}PNP iridium ethyl hydride complex **3d** $\Delta G°$ is predicted to be +15.6 kcal/mol ($\Delta H°$ = 28.9 kcal/mol), representing a very pronounced difference of 18 kcal/mol for C−H elimination/addition. The barrier to reductive C−H coupling in **3d** is calculated as $\Delta G^{‡}$ = 16.6 kcal/mol (Figure 4); this coupling leads to a C−H σ-bond complex, **3e**, with free energy 22.1 kcal/mol above ethylene dihydride complex **3c**. The ethane molecule in **3e** is bound quite strongly; $\Delta H°$ for dissociation to yield **3f** is 11.9 kcal/mol.

We have not been able to locate a proper TS on the potential energy surface for dissociation of ethane from the C−H σ-bond complex **3e**, but we can provide an estimate for the effective free energy barrier. We assume that $\Delta H^{‡} \approx$ 11.9 kcal/mol (equal to $\Delta H°$, and thus presumably a lower limit since this assumes that $\Delta H^{‡}$ = 0 for the back reaction) and that $\Delta S^{‡}$ for this unimolecular, dissociative, process is in the range of 10−20 eu. These assumptions yield a range of values for $\Delta G^{‡}$ for ethane loss from **3e** at 25 °C of 5.9 to 8.9 kcal/mol or, in effect, a TS with free energy from 28 to 31 kcal/mol above that of resting state **3c**.

At 75 °C, the temperature at which the $[C_2H_4]$ dependence was experimentally determined, the resulting rate equation (eq 8) indicates a first-order rate constant of 1.3×10^{-4} s^{-1} for **3c** undergoing overall ethylene insertion and ethane loss; this rate corresponds to $\Delta G^{‡}_{exp}$ = 26.7 kcal/mol. At this temperature, the calculated free energy of ethane complex **3e** is 21.7 kcal/mol above **3c** (the value is 22.1 kcal/mol at 25 °C). Again assuming that $\Delta H^{‡} \approx$ 11.9 kcal/mol for ethane loss from **3e** and $\Delta S^{‡}$ = 10−20 eu, the estimated free energy (relative to **3c**) of the effective TS for ethane loss is 33.6 kcal/mol (21.7 kcal/mol +11.9 kcal/mol) minus 3.5−7.0 kcal/mol (10−20 eu at 75 °C); this is equal to 26.6−30.1 kcal/mol, in full agreement with the experimental value of 26.7 kcal/mol.

2.4.2.2. The Ethylene-Assisted (Associative) Pathway. Addition of ethylene to ethyl hydride **3d**, can give two isomers, **3d-*cis*-C_2H_4** and **3d-*trans*-C_2H_4**, where the ethylene and ethyl groups are mutually *cis* or *trans*, respectively, with free energies 2.2 and 4.3 kcal/mol above that of **3d** plus free ethylene. A proper TS for the addition was not located, but incremental scans of the potential energy surfaces reveal that both additions proceed with virtually no energy barrier. The free energy of the TS (or the effective TS) may be estimated using the same procedure as outlined above for dissociation of ethane from **3e** (in this case proceeding in the reverse direction). The enthalpy of ethylene loss from **3d-*trans*-C_2H_4** is calculated to be 11.9 kcal/mol (coincidentally equal to the value for ethane loss

dx.doi.org/10.1021/ja501572g | J. Am. Chem. Soc. 2014, 136, 6672−6683

from **3e**); if $\Delta S^{\ddagger}$ is again estimated to be in the range of 10−20 eu, then $\Delta G^{\ddagger}$ lies in the range 5.9−8.9 kcal/mol, which places the TS (for ethylene loss from **3d-*trans*-C_2H_4** or ethylene addition to **3d**) at ∼16−19 kcal/mol above the resting state **3c** plus ethylene at 25 °C (Figure 4). Elimination from **3d-*cis*-C_2H_4** is calculated to be slightly less favorable, with a TS about 5 kcal/mol higher than that for elimination from **3d-*trans*-C_2H_4**.

Reductive elimination from six-coordinate d^6 complexes is generally not a facile process,[41] and indeed $\Delta G^{\ddagger}$ for elimination from **3d-*trans*-C_2H_4** is substantial, 16.0 kcal/mol at 25 °C, with a TS (**TS-3d/3a**) that is 26.4 kcal/mol above the free energy of **3c** plus ethylene (1 atm) (Figure 4). At 75 °C, the value is 28.9 kcal/mol at 1 atm ethylene or 26.5 kcal/mol at 1 mol/L (28 atm), in excellent agreement with the second-order rate constant of 7.2×10^{-4} M^{-1} s^{-1} obtained at this temperature (eq 8) which corresponds to $\Delta G^{\ddagger}_{exp}$ = 25.5 kcal/mol. Metric parameters for the isomeric TS's for ethylene-assisted ethane elimination are shown in Scheme 5.

Scheme 5. TS for Elimination of Ethane from 3d-*trans*-C_2H_4 and from 3d-*trans*-C_2H_4 (TS-3d/3a)[a]

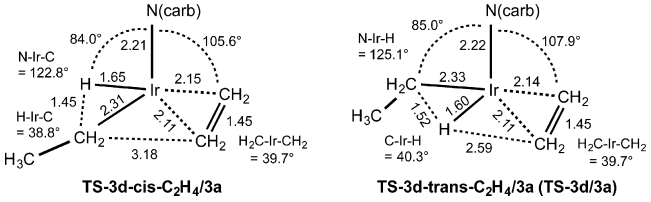

[a]Metrics are shown (bond lengths in Å) for the coordination sphere excluding the coordinating P atoms (i.e., for the ligands in the approximate plane bisecting the P−Ir−P axis).

Reductive elimination of ethane from **3d-*trans*-C_2H_4** is strongly exergonic (ΔG° = −21.6 kcal/mol) in striking contrast with the value obtained for elimination from five-coordinate ethyl hydride **3d**, ΔG° = +15.6 kcal/mol. The TS for the uphill reductive coupling by **3d** is, however, calculated to be somewhat lower than reductive coupling by **3d-*trans*-C_2H_4**. Reductive elimination (i.e., loss of ethane), however, is significantly less favorable from **3d**. This can be explained in terms of the free energy of reductive coupling (ΔG° = 15.0 kcal/mol) to give **3e**, combined with the thermodynamic barrier to loss of ethane from ethane complex **3e** (ΔH° = 11.9 kcal/mol). Alternatively, and perhaps most simply, the barrier may be explained by considering the high endothermicity of ethane loss from **3d**; ΔH° = +28.9 kcal/mol (or +36.7 kcal/mol relative to resting state **3c**). Even a total entropic contribution as great as ΔS = +30 eu in the rate-determining step only lowers $\Delta G^{\ddagger}$ to ca. 28 kcal/mol above **3c**. Consequently, it is ultimately the unfavorable thermodynamics (specifically the high positive enthalpy) that results in a very high kinetic barrier for the unassisted elimination. In the case of the ethylene assisted pathway, the overall thermodynamics of elimination (driven by ethylene coordination) are quite favorable. Thus, while there is a fairly high kinetic barrier to elimination from six-coordinate **3d-*trans*-C_2H_4**, in the presence of ethylene (ca. 1 atm or greater) the associative pathway is still the more favorable one with $\Delta G^{\ddagger}$ = 26.4 kcal/mol relative to **3c**, in excellent agreement with the experimentally determined dependence of rate on the concentration of ethylene (eq 8).

*2.4.3. Reaction of Ethyl Hydride **3d** under a H_2 Atmosphere.* The experimental kinetics indicate that an H_2-assisted pathway for the release of ethane from ethylene dihydride complex **3c** is even more favorable than the ethylene-assisted pathway. The DFT calculations strongly support this conclusion. As discussed above, the unassisted pathway (involving dissociative loss of ethane from **3d**) appears to have a free energy barrier (25 °C) of ca. 28 kcal/mol relative to resting state **3c** or 22 kcal/mol above ethyl hydride **3d**. In the presence of an H_2 atmosphere, the five-coordinate unsaturated ethyl hydride complex **3d** is calculated to add H_2 with no barrier on the energy surface (just as it readily adds ethylene), to afford a dihydrogen complex with the dihydrogen ligand *trans* or *cis* to the ethyl group (**3d-*trans*-(H_2)** or **3d-*cis*-(H_2)**, respectively); coincidentally, either species has a free energy 4.9 kcal/mol above that of **3c** (Figure 5). If $\Delta H^{\ddagger} \sim \Delta H^{\circ} \sim 11$ kcal/mol for the reverse reaction (loss of dihydrogen from **3d-*trans*-(H_2)** or **3d-*cis*-(H_2)**) and if $\Delta S^{\ddagger}$ is estimated to be in the range of 10−20 eu, then the effective TS for the H_2 elimination/addition has a free energy of 10−13 kcal above **3c**. This corresponds to a free energy of 4−7 kcal/mol above that of **3d**, which is fully consistent with an approximately diffusion-controlled reaction (e.g., a diffusion-controlled rate of ca. 10^{10} M^{-1} s^{-1};[42] and a concentration of 0.041 M H_2, equivalent to 1 atm, corresponds to a pseudo-first-order rate constant of 4×10^8 s^{-1} and $\Delta G^{\ddagger}$ = 5.7 kcal/mol at 25 °C).

3d-*trans*-(H_2) readily converts to an Ir(V) species **3g** (with ΔG° = 1.0 kcal/mol) in a nearly barrierless transition. The TS for this conversion, **TS-A**, is a mere 0.7 kcal/mol higher in electronic energy, *E*, than **3g**. Species **3g**, although a minimum on the electronic energy surface, is actually slightly higher than **TS-A** in free energy and even enthalpy. It is thus questionable whether **3g** can even be characterized as a true intermediate. Importantly, however, no matter whether it is a minimum or a nonstationary point on the reaction coordinate, the Ir(V) species **3g** connects to Ir(III) species **3b** via **TS-B** to lose ethane; the barrier to this transformation is only 2.0 kcal/mol (Figure 5). Scheme 6 illustrates the geometry of these species along the reaction coordinate. The full Ir(V) character of **3g** is clear from the absence of any close interhydride or carbon-hydride contacts. It can be seen that the reaction coordinate (**3d-*trans*-(H_2)** → **TS-A** → **3g** → **TS-B** → **3b** + C_2H_6) is comprised almost exclusively of H_b moving away from H_a combined with movement of H_c toward the α-carbon of the ethyl group. These motions occur concomitantly although the motion of H_b is somewhat more pronounced at earlier points on the reaction coordinate (cf. **TS-A** and **3g**), while the motion of H_c is somewhat more pronounced later (cf. **3g** and **TS-B**).

In the pathway calculated to be most favorable for the H_2-assisted C−H elimination, the hydrogen undergoing C−H elimination (H_c in Scheme 6) is derived from the hydride ligand of **3d**, rather than from the incoming H_2 molecule. A pathway in which the ethane hydrogen is derived from the incoming H_2 was calculated, but its TS for elimination (**TS-C**) has a free energy of 17.5 kcal/mol which, though not prohibitively high, is significantly above that of **TS-B** (7.9 kcal/mol). **TS-C** might be viewed as being a point on a σ-CAM (σ-complex assisted metathesis) pathway.[43] Note that although **TS-C** is higher in energy than **TS-B**, the σ-CAM-type pathway is apparently not intrinsically unfavorable. In fact, **TS-C** is calculated to be slightly lower in energy than **TS-D**, a C−H elimination TS which, like **TS-C**, connects to **3d-*cis*-(H_2)** but in **TS-D** the eliminating H atom is derived from a hydride ligand of **3b**. (Thus, of the two pathways examined for H_2-assisted C−H

dx.doi.org/10.1021/ja501572g | J. Am. Chem. Soc. 2014, 136, 6672−6683

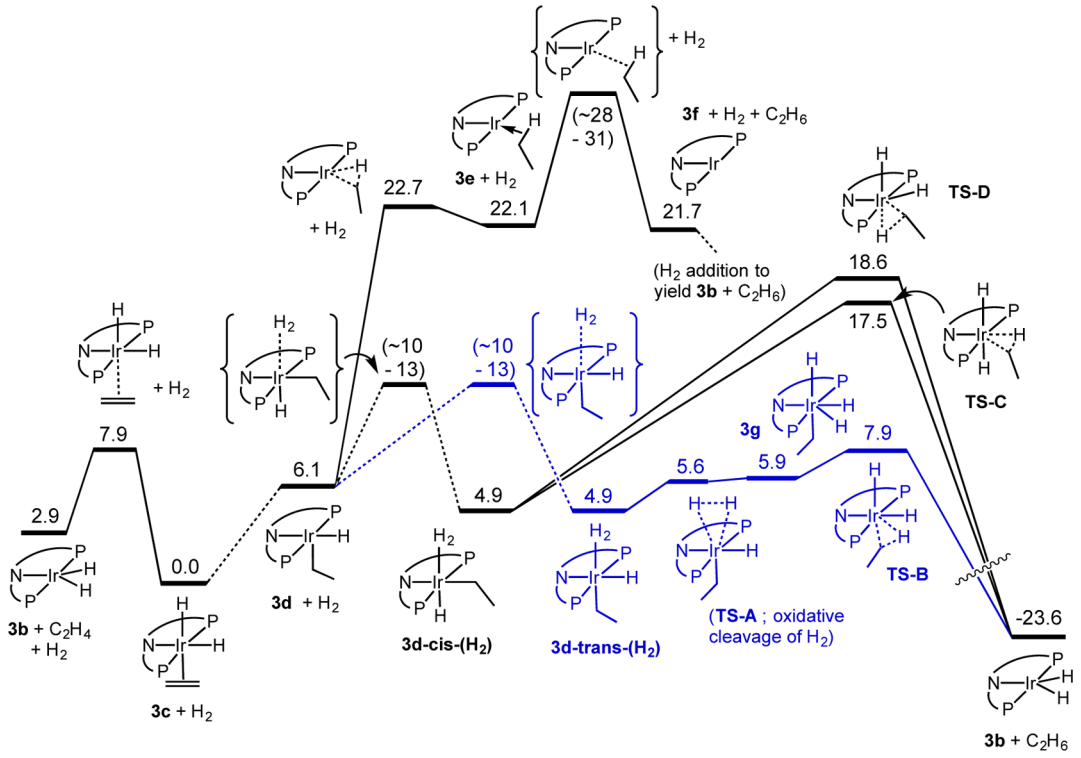

Figure 5. Calculated free energies (kcal/mol) for hydrogenation of ethylene by **3b** under 1 atm H_2 (favored path in blue). Structures in brackets ({ }) are not calculated geometries; they are shown to illustrate the barriers estimated (see explanation in text) for steps which do not appear to proceed via a TS.

Scheme 6. Species on the Reaction Pathway From 3d-*trans*-(H_2) to Dihydride 3b[a]

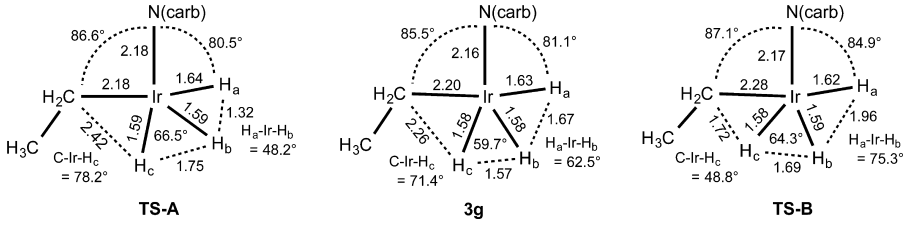

[a]Metrics are shown (bond lengths in Å) for the coordination sphere excluding the coordinating P atoms (i.e., for the ligands in the approximate plane bisecting the P−Ir−P axis).

elimination from the intermediate **3d-*cis*-(H_2)**, the σ-CAM pathway is the slightly more favorable).

It is interesting to note that (PONOP)Ir(CH_3)(H)$^+$ (PONOP =2,6-bis(di-*tert*-butylphosphinito)pyridine), isoelectronic with **3d**, adds H_2 to form dihydrogen adduct (PONOP)Ir(CH_3)(H)-(η^2-H_2)$^+$, which can be observed by low-temperature NMR spectroscopy.[44] The H_2 ligand is *trans* to the terminal hydride. Elimination of methane from (PONOP)Ir(CH_3)(H)$^+$ occurs by a σ-CAM mechanism in which the hydrogen that is eliminated originates from the η^2-H_2 ligand in analogy to the conversion of **3d-*cis*(H_2)** to **3b** plus C_2H_6 via **TS-C**. The barrier to elimination from the dihydrogen complex (PONOP)Ir(CH_3)(H)(η^2-H_2)$^+$ is significantly lower (17.9 kcal/mol) than the direct elimination of methane from methyl hydride (PONOP)Ir(CH_3)(H)$^+$, consistent with DFT computations for the carbazolide analogue in Figure 5.

The comparison of the H_2-assisted path for ethane elimination with the ethylene-assisted path is informative (Figures 4 and 5; summary in Figure 6). Addition of either H_2 or ethylene to ethyl hydride **3d** proceeds without any significant kinetic or thermodynamic barrier. Both of the resulting adducts are coordinatively saturated 18-valence-electron complexes. Since the ethane product is derived from the ethyl and hydride ligands of **3d**, not from the incoming dihydrogen molecule, the H_2-assisted pathway can be viewed as a displacement reaction in analogy with the reaction with ethylene. Elimination from the six-coordinate d^6 ethylene adducts, however, has a substantial kinetic barrier, ca. 16 kcal/mol in the most favorable case, reflecting the general and well-explained[45] behavior of such species. In contrast, upon addition of H_2, the barrier to ethane loss is quite low. This may be attributed to the ability of the added H_2 (in contrast with ethylene) to undergo oxidative cleavage to give an Ir(V) species.

In either the reaction with ethylene or with H_2, the elimination of ethane following the addition is very exothermic. In the case of the ethylene-assisted reaction, inspection of the TS (**TS-3d/3a** shown in Scheme 7) as well as the IRC reveals that as the ethane dissociates from the complex the geometry of the remaining coordination sphere is severely distorted from the square-planar geometry of the final product in which

dx.doi.org/10.1021/ja501572g | J. Am. Chem. Soc. 2014, 136, 6672−6683

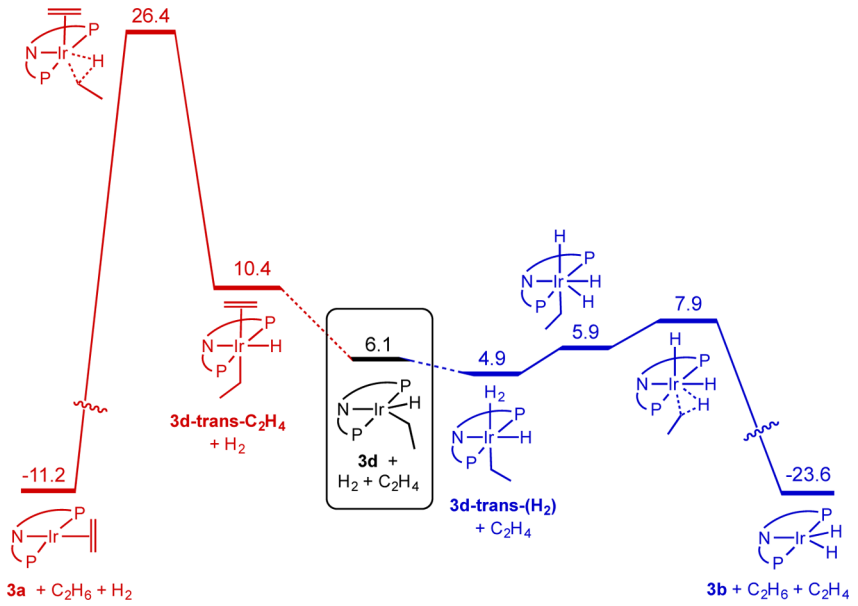

Figure 6. Comparison of ethane elimination from **3d** promoted by addition of H_2 (blue) and promoted by addition of ethylene (red).

Scheme 7

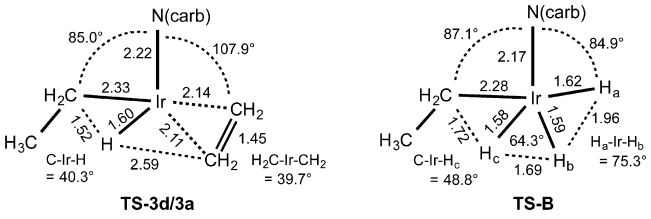

ethylene is *trans* to nitrogen. (This reflects Hoffmann's explanation for the barrier to reductive elimination from such species.) In contrast, in the case of the H_2 adduct (see **TS-B**, Scheme 7), C−H bond formation smoothly leads to formation of a d^6 octahedral ethane complex with H_b *trans* to N and H_a *trans* to ethane. This is followed by a presumably barrierless dissociation of ethane to afford a low-energy square-pyramidal species (with H_a apical, and H_b *trans* to N) which is analogous to the microscopic reverse of the barrierless addition of H_2 to five-coordinate ethyl hydride **3d**.

While **3g** is calculated to be an Ir(V) intermediate complex preceding **TS-B** on the reaction coordinate, one might envision a pathway without any such energy minimum along the reaction coordinate, in which ethane elimination proceeds concertedly with H−H oxidative cleavage. But regardless, the barrier for the H_2-assisted pathway is extremely facile because of the low energy of species (intermediates and/or TS's) that are clearly Ir(V) in character; it is these species that allow a nearly barrierless transition from the dihydrogen adduct of the ethyl hydride (**3d-*trans*-H2**) reactant, to the ethane adduct of the dihydride product.

Thus, the unassisted elimination of ethane has a high barrier attributable to the thermodynamic unfavorability of three-coordinate Ir(I) relative to Ir(III) in the case of the carbazolide−PNP complex. The ethylene-assisted pathway has a somewhat lower barrier (ca. 26 kcal/mol) attributable to the kinetics of interconversion between octahedral Ir(III) and square-planar Ir(I). The H_2-assisted pathway faces neither of these difficulties. Accordingly, the kinetics of the H_2-assisted pathway are apparently limited only by the kinetics of formation of **3d** (i.e., insertion of ethylene into the Ir−H bond of **3c**), and it thus proceeds at a rate comparable to H/D exchange by **3c**−$\mathbf{d_2}$.

3. DISCUSSION AND SUMMARY

The much poorer σ-donating ability of the central nitrogen atom (relative to the central carbon atom of iridium PCP and iridium POCOP systems) in the iridium carbazolide system studied here gives rise to a stronger preference for the Ir(III) oxidation state, relative to Ir(I), for the carbazolide system. For example, the enthalpy of ethane loss from five-coordinate ethyl hydride **3d** is calculated to be 28.9 kcal/mol vs only 10.1 kcal/mol from (^{iPr}PCP)Ir(H)Et. The free energy of **3d** is calculated as 6.1 kcal/mol above that of the six-coordinate ethylene *cis*-dihydride resting state, **3c**, and thus the overall barrier to "unassisted" release of ethane from **3c** is quite high.

The high barrier to ethane elimination from **3d** results in unusual features with respect to hydrogenation of olefins by these complexes. The (^{carb}PNP)Ir dihydride, **3b**, readily adds ethylene to give **3c**. This is rapidly followed by olefin insertion to give the ethyl hydride, **3d**, as shown by rapid H/D exchange between hydride ligands and ethylene hydrogens. Although direct elimination of ethane from **3d** has a very high barrier, **3d** can easily trap ethylene. The resulting six-coordinate adduct, specifically the isomer **3d-*trans*-$\mathbf{C_2H_4}$**, has a significant kinetic barrier to elimination ($\Delta G^{\ddagger}$ = 16 kcal/mol). Nevertheless the overall calculated barrier of 26.4 kcal/mol is less than that predicted for a direct ethane elimination pathway, and indeed the absolute value of this barrier and the predicted dependence on ethylene pressure is in excellent agreement with the experimental rate and the kinetic dependence on ethylene pressure. A similar "ethylene-promoted" reductive elimination from the facially substituted cationic iridium complex $L_3IrH_2(C_2H_4)^+$ (L = $PPhMe_2$) has been noted by Caulton.[46]

The effect of hydrogen on lowering the overall barrier to hydrogenation of ethylene by **3c** is much more pronounced than the effect of ethylene. DFT calculations suggest that the ethyl hydride adds H_2 to form the η^2-dihydrogen complex, **3d-*trans*-($\mathbf{H_2}$)**; this barrierless step is followed by rapid reductive elimination of ethane proceeding via an Ir(V) intermediate, with an extremely low overall barrier, $\Delta G^{\ddagger}$ = 3 kcal/mol. This

dx.doi.org/10.1021/ja501572g | J. Am. Chem. Soc. 2014, 136, 6672−6683

lower barrier for reductive elimination relative to the ethylene-promoted pathway may be explained in terms of the carbazoleide pincer engendering a strong preference for the Ir(III) oxidation state vs Ir(I), the lack of any species with Ir(I) character along the reaction coordinate, and the fact that there is no net change in the oxidation state upon release of ethane from the dihydrogen complex, **3d**-H_2.

Experimental and computational studies suggest that cationic LL′Ir$^+$ Crabtree-type hydrogenation catalysts[47] can function via Ir(III)/Ir(V)/Ir(III) cycles. Brandt et al.[48] carried out computational and experimental studies on a cationic phosphanooxazoline iridium catalyst[49] that supported an olefin hydrogenation cycle in which an unsaturated Ir(III) olefin dihydride species is the catalyst resting state; hydrogenation proceeds via addition of H_2 to form an Ir(III) olefin η^2-dihydrogen dihydride complex, followed by migratory insertion and oxidative cleavage of the dihydrogen ligand to yield an Ir(V) alkyl trihydride. Facile elimination of alkane from this Ir(V) species followed by coordination of olefin closes the catalytic cycle. Similar conclusions were reached by Cui et al.[50] in their study of cationic Ir(III) hydrogenation catalysts employing bidentate N-heterocyclic carbene-oxazoline ligands. In a study of the hydrogenation of ethylene by (triphos)Ir$(C_2H_4)_2^+$ Bianchini has suggested that both ethylene and H_2 can accelerate the reductive elimination of ethylene based on the half-order pressure dependence of both hydrogen and ethylene on the rate of hydrogenation.[51]

The hydrogen-induced acceleration of olefin hydrogenation by dihydride **3b** is even more dramatic in the case of more hindered olefins. Neither propylene nor TBE form stable adducts with **3b** and neither react with **3b** to give alkane even at temperatures up to 100 °C. Deuterium labeling shows that olefin binding and insertion occurs, and alkyl hydrides are readily formed reversibly at rt, but apparently even at 100 °C the barrier to reductive elimination is too high to complete the hydrogenation reaction. These olefins, however, are rapidly hydrogenated at rt under hydrogen, presumably via addition of hydrogen to the corresponding alkyl hydride complex.

Our studies of the hydrogenations explain why the carbazoleide complex is ineffective for catalytic transfer dehydrogenation. Under transfer dehydrogenation conditions there is no free hydrogen present, and thus the required hydrogenation step in the cycle has an exceptionally high barrier. In comparison with the much more effective PCP-type pincer complexes, the difference is ultimately attributable to the very unfavorable thermodynamics of the Ir(III) → Ir(I) transformations, particularly elimination of alkane from the five-coordinate alkyl hydride **3d** (the high barrier may also be expressed in terms of the very unfavorable thermodynamics of transfer of hydrogen from the Ir(III) dihydride to olefin). Notably, preference for the higher oxidation state is in turn attributable to the much poorer σ-donating ability of the carbazolide nitrogen relative to that of the coordinating carbon of the PCP-type pincers. As the carbazolide ligand biases the system strongly in favor of the +3 vs +1 oxidation state, future work with this ligand will focus on rhodium, since, in the case of PCP-type pincer ligands, the Rh(III) state is not sufficiently accessible to allow an effective catalytic cycle based on the Rh(I)/Rh(III) couple.

4. EXPERIMENTAL SECTION

4.1. General Comments. All manipulations were carried out using standard Schlenk, high-vacuum, and glovebox techniques. Argon was purified by passing through columns of BASF R3-11 catalyst (Chemalog) and 4 Å molecular sieves. All chemicals were purchased from commercial sources and used without purification unless otherwise stated. $[Ir(C_2H_4)_2Cl]_2$ and **6** were prepared as described.[29,52] NMR spectra were recorded on Bruker NMR spectrometers (AV-400, DRX-500, and AV-600). ^{1}H and ^{13}C{^{1}H} NMR spectra were referenced to residual solvent peaks. ^{31}P{^{1}H} NMR spectra were referenced to 85% aqueous H_3PO_4 except for spectra obtained below 0 °C. For species in which two *trans* phosphorus atoms exhibited strong coupling, virtual triplets were observed.

4.2. Synthesis of 3,6-Dimethyl-9*H*-carbazole-1,8-dicarboxylic Acid (7). To a solution of **6** (2.48 g, 7.02 mmol) in diethyl ether (100 mL) was added ^{n}BuLi (3.0 mL, 2.5 M in hexane, 7.5 mmol) at 0 °C. After stirring for 1 h at 0 °C, Me_3SiCl (0.98 mL, 7.7 mmol) was added, and the reaction mixture was allowed to warm to 23 °C. After stirring at this temperature for 1 h, the suspension was cooled to −78 °C, and ^{t}BuLi (19 mL, 1.6 M in pentane, 30 mmol) was added slowly. The reaction mixture was stirred at 0 °C for 3 h. At −78 °C, the reaction mixture was exposed to a CO_2 atmosphere and allowed to warm to 23 °C overnight. Hydrolysis was performed at 0 °C by the addition of aqueous HCl (50 mL, 1 N). The organic product was extracted with ethyl acetate, washed with aqueous NaCl (2 × 100 mL, 3 M), dried over anhydrous $MgSO_4$, and filtered, and the solvent was evaporated. The residue solid was washed with diethyl ether (2 × 5 mL) to afford the product as a light-yellow solid (1.7 g, 6.0 mmol, 86% yield). ^{1}H NMR (400 MHz, DMSO): δ 10.91 (s, 1H, NH), 8.23 (s, 2H, Ar−H), 7.85 (s, 2H, Ar−H), 2.51 (s, 6H, Ar−CH_3). ^{13}C NMR (150 MHz, DMSO): δ 167.98, 137.88, 128.97, 128.25, 125.93, 123.41, 112.55, 20.86. MS (EI) m/z: 283.08 (calcd: 283.08).

4.3. Synthesis of (3,6-Dimethyl-9*H*-carbazole-1,8-diyl)dimethanol (8). To a solution of **7** (1.0 g, 3.5 mmol) in dry THF (30 mL) at −78 °C was added $LiAlH_4$ (500 mg, 13.2 mmol). The reaction mixture was allowed to warm to 23 °C and then heated at 70 °C for 2 h. The excess $LiAlH_4$ was quenched with aqueous NaOH (15%, 3 mL) under vigorous stirring, and the reaction mixture was filtered over a layer of Celite. The solvent was evaporated, and the residue was dissolved in diethyl ether, washed with H_2O, dried over $MgSO_4$, and filtered, and the solvent was evaporated to afford the product as a light yellow solid (0.77 g, 3.0 mmol, 85% yield). ^{1}H NMR (400 MHz, DMSO): δ 10.29 (s, 1H, NH), 7.73 (s, 2H, Ar−H), 7.17 (s, 2H, Ar−H), 5.25 (t, J = 5.65 Hz, OH), 4.85 (d, J = 5.65 Hz, CH_2), 2.45 (s, 6H, Ar−CH_3). ^{13}C NMR (150 MHz, DMSO): δ 136.40, 127.32, 125.41, 125.25, 123.03, 118.84, 60.79 (CH_2), 21.62 (Ar−CH_3). Anal. calcd for $C_{16}H_{17}NO_2$: C, 75.27; H, 6.71; N, 5.49. Found: C, 73.53; H, 6.46; N, 4.95.

4.4. Synthesis of 1,8-Bis(bromomethyl)-3,6-dimethyl-9*H*-carbazole (9). To a solution of **8** (0.50 g, 2.0 mmol) in dry THF (10 mL) was added PBr_3 (1.0 mL, 2.9 g, 10 mmol) at 0 °C. The reaction mixture was stirred at 0 °C for 3 h and then poured into H_2O (100 mL) at 0 °C. The organic product was extract with ether, washed with H_2O, dried over $MgSO_4$, and filtered, and the solvent was evaporated to afford the product as a yellow solid (0.65 g, 1.7 mmol, 87% yield). ^{1}H NMR (500 MHz, C_6D_6) δ 8.36 (s, 1H, NH), 7.62 (s, 2H, Ar−H), 6.78 (s, 2H, Ar−H), 4.26 (s, 4H, CH_2), 2.29 (s, 6H, Ar−CH_3). ^{13}C NMR (151 MHz, C_6D_6) δ 137.59, 129.10, 127.88, 124.94, 121.64, 119.91 (s), 31.22 (s, CH_2), 21.20 (s, Ar−CH_3). Anal. calcd for $C_{16}H_{15}Br_2N$: C, 50.42; H, 3.97; N, 3.68. Found: C, 51.77; H, 4.28; N, 3.61.

4.5. Synthesis of 1,8-Bis((diisopropylphosphino)methyl)-3,6-dimethyl-9*H*-carbazole (1). To a solution of **9** (0.38 g, 1.0 mmol) in degassed CH_2Cl_2 (20 mL) was added HP(^{i}Pr)$_2$ (0.26 g, 2.2 mmol) at 23 °C. The reaction mixture was stirred at 23 °C for 4 h, and the solvent was evaporated. The residue was washed with pentane (3 × 10 mL) and redissolved in CH_2Cl_2 (20 mL). To this solution was added Et_3N (1.0 mL, 0.73 g, 7.2 mmol). After stirring at 23 °C for 15 min, the volatiles were evaporated, the residue extracted with diethyl ether, filtered, and diethyl ether was evaporated to afford the product as a light yellow solid (0.41 g, 0.90 mmol, 90% yield). ^{1}H NMR (400 MHz $CDCl_3$): 9.04 (s, 1H, NH), 7.65 (s, 2H, Ar−H), 7.07 (s, 2H, Ar−H), 3.09 (s, 4H, CH_2), 2.49 (s, 6H, Ar−CH_3), 1.85−1.79 (m, 4H, CH(CH_3)$_2$), 1.15−1.07 (m, 24H, CH(CH_3)$_2$). ^{13}C NMR

dx.doi.org/10.1021/ja501572g | J. Am. Chem. Soc. 2014, 136, 6672−6683

(100 MHz $CDCl_3$): 137.70, 128.57, 127.77, 124.04, 121.82, 117.92, 26.58 (d, J_{CP} = 20.2 Hz, CH2), 23.71 (d, J_{CP} = 13.5 Hz, $CH(CH_3)_2$), 21.56 (s, Ar−CH_3), 19.77 (s, $CH(CH_3)_2$), 19.36 (s, $CH(CH_3)_2$). ^{31}P NMR (162 MHz, $CDCl_3$) δ 0.43 (s). Anal. calcd for $C_{28}H_{43}NP_2$: C, 73.82; H, 9.51; N, 3.07. Found: C, 73.10; H, 8.98; N, 3.13.

4.6. Synthesis of 1,8-Bis((diisopropylphosphino)methyl)-3,6-dimethylcarbazolide Iridium(I) Ethylene (3a). To a solution of **9** (0.16 g, 0.36 mmol) in benzene (10 mL) was added slowly $LiN(TMS)_2$ (61 mg, 0.36 mmol) at 23 °C, and the solution turned dark red instantly. After stirring for 5 min, a solution of $[(C_2H_4)_2IrCl]_2$ (0.10 g, 0.36 mmol) in benzene (5 mL) was added to the reaction mixture. After stirring for 5 min, the reaction mixture was filtered, and the volatiles were evaporated to afford **3a** as a dark-brown solid (0.19 g, 0.28 mmol, 78%). ^1H NMR (600 MHz, Tol) δ 7.90 (s, 2H, Ar−H), 6.83 (s, 2H, Ar−H), 2.94 (vt, J_{PH} = 3.3 Hz, 4H, CH_2), 2.58 (s, 6H, Ar−CH_3), 1.87−1.79 (m, 4H, $CH(CH_3)_2$), 1.76 (vt, J_{PH} = 5.0 Hz, 4H, C_2H_4), 1.04 (dd, J = 14.1, 7.1 Hz, 12H, $CH(CH_3)_2$), 0.94 (dd, J = 12.8, 6.4 Hz, 12H, $CH(CH_3)_2$). ^{13}C NMR (151 MHz, Tol) δ 149.67 (vt, J_{CP} = 4.2 Hz), 127.46 (vt, J_{CP} = 3.5 Hz), 126.27 (s), 126.17 (s), 121.48 (s), 119.32 (s), 23.59 (vt, J_{CP} = 12.9 Hz, $CH(CH_3)_2$), 21.84 (s, Ar−CH_3), 19.80 (s, CH_2), 19.04 (s, $CH(CH_3)_2$), 18.09 (s, $CH(CH_3)_2$), 16.32 (s, C_2H_4). ^{31}P NMR (243 MHz, Tol) δ 30.80 (s). Anal. calcd for $C_{30}H_{46}IrNP_2$: C, 53.39; H, 6.87; N, 2.08. Found: C, 53.89; H, 7.01; N, 1.81.

4.7. Observation of 1,8-Bis((diisopropylphosphino)methyl)-3,6-dimethylcarbazolide Iridium(III) Dihydride (3b). Hydrogen was purged through a solution of **3a** (5 mg, 0.07 mmol) in toluene-d_8 (0.5 mL) for 15 min. The product formed quantitatively. ^1H NMR (600 MHz, Tol) δ 7.90 (s, 2H, Ar−H), 6.91 (s, 2H, Ar−H), 3.08 (t, J = 3.1 Hz, 4H, CH_2), 2.57 (s, 6H, Ar−CH_3), 1.80−1.69 (m, 4H, $CH(CH_3)_2$), 0.99 (dd, J = 13.9, 6.9 Hz, 12H, $CH(CH_3)_2$), 0.91 (dd, J = 14.6, 7.2 Hz, 12H, $CH(CH_3)_2$), −28.14 (t, J = 12.7 Hz, 2H, IrH). ^{13}C NMR (151 MHz, Tol) δ 149.25 (s), 128.44 (s), 127.08 (s), 126.59 (s), 122.75 (s), 119.76 (s), 26.30 (t, J = 16.0 Hz, $CH(CH_3)_2$), 22.57 (t, J = 11.2 Hz, CH_2), 21.95 (s, Ar−CH_3), 19.43 (s, $CH(CH_3)_2$), 19.10 (s, $CH(CH_3)_2$). ^{31}P (243 MHz, Tol): 57.03 (s).

4.8. Observation of 1,8-Bis((diisopropylphosphino)methyl)-3,6-dimethylcarbazolide Iridium(III) Ethylene *cis*-Dihydride (3c). Ethylene was purged through a solution of **3b** (6.7 mg, 0.010 mmol) in toluene-d_8 (0.5 mL) at −50 °C for 1 min, and the product formed quantitatively. ^1H NMR (500 MHz, Tol, −50 °C) δ 7.98 (s, 2H, Ar−H), 6.97 (s, 2H, Ar−H), 3.15−3.00 (m, 4H, CH_2), 2.73 (s, 6H, Ar−CH_3), 1.88 (s, 4H, C_2H_4), 1.86−1.80 (m, 2H, $CH(CH_3)_2$), 1.77−1.71 (m, 2H, $CH(CH_3)_2$), 1.00−0.88 (m, 18H, $CH(CH_3)_2$), 0.77 (dd, J = 14.1, 7.1 Hz, 6H, $CH(CH_3)_2$), −11.83 (td, J = 18.2, 5.2 Hz, 1H, IrH), −23.99 (td, J = 13.6, 5.8 Hz, 1H). ^{13}C NMR (126 MHz, Tol, −50 °C) δ 150.31 (s), 127.29 (s), 126.76 (s), 123.92 (s), 120.47 (s), 119.73 (s), 50.83 (s, C_2H_4), 26.81 (t, J = 12.9 Hz, CH_2), 25.58 (t, J = 15.7 Hz, $CH(CH_3)_2$), 23.96 (t, J = 18.2 Hz, $CH(CH_3)_2$), 23.01 (s, $CH(CH_3)_2$), 22.55 (s, Ar−CH_3), 20.64 (s, $CH(CH_3)_2$), 18.86 (s, $CH(CH_3)_2$), 16.97 (s, $CH(CH_3)_2$). ^{31}P NMR (202 MHz, Tol, −50 °C) δ 43.37 (bs).

5. COMPUTATIONAL DETAILS

Most computational data quoted in the main text result from DFT calculations employing the M11 exchange−correlation functionals;[32] the Ir SDD relativistic effective core potential and associated (6s5p3d) valence basis set;[53] and 6-311G(d,p) basis sets on all other atoms (P, N, C, and H).[54] The bulky *i*Pr groups on P were retained in the computations. Enthalpies (H^o) and Gibbs' free energies (G^o; T = 298.15 K, P = 1 atm) were obtained from the electronic potential energies (E) using standard statistical mechanical expressions applicable to the harmonic oscillator/rigid rotor approximations.

In the Supporting Information, we present energetic results in the form of three tables. Tables S1 and S2 contain relative energies pertinent to Figures 4 and 5 in the main text, respectively; and Table S3 provides absolute energies for relevant minima and transition states. Additional computational details are also available in Supporting Information.

■ ASSOCIATED CONTENT

Ⓢ Supporting Information

Kinetic data, computational details, tables of thermodynamic quantities (E, H, G, S) and optimized geometries, absolute energies, structural depictions and .mol files of species relevant to Figures 4 and 5. This material is available free of charge via the Internet at http://pubs.acs.org.

■ AUTHOR INFORMATION

Corresponding Authors

mbrookhart@unc.edu
kroghjes@rutgers.edu
alan.goldman@rutgers.edu

Present Address

[§]Department of Chemistry Education and Research Institute of Natural Science, Gyeongsang National University, 660−701 Jinju, Republic of Korea.

Notes

The authors declare no competing financial interest.

■ ACKNOWLEDGMENTS

This work was supported by the NSF through the CCI Center for Enabling New Technologies through Catalysis (CENTC) Phase II Renewal, CHE-1205189.

■ REFERENCES

(1) Findlater, M.; Choi, J.; Goldman, A. S.; Brookhart, M. *Catal. Met. Complexes* **2012**, *38*, 113−141.

(2) Choi, J.; MacArthur, A. H. R.; Brookhart, M.; Goldman, A. S. *Chem. Rev.* **2011**, *111*, 1761−1779.

(3) Huang, Z.; Brookhart, M.; Goldman, A. S.; Kundu, S.; Ray, A.; Scott, S. L.; Vicente, B. C. *Adv. Synth. Catal.* **2009**, *351*, 188−206.

(4) Morales-Morales, D. *Iridium Complexes Org. Synth.* **2009**, 325−344.

(5) Xu, W.; Rosini, G. P.; Gupta, M.; Jensen, C. M.; Kaska, W. C.; Krogh-Jespersen, K.; Goldman, A. S. *Chem. Commun.* **1997**, 2273−2274.

(6) Goldman, A. S.; Roy, A. H.; Huang, Z.; Ahuja, R.; Schinski, W.; Brookhart, M. *Science* **2006**, *312*, 257−261.

(7) Nawara-Hultzsch, A. J.; Hackenberg, J. D.; Punji, B.; Supplee, C.; Emge, T. J.; Bailey, B. C.; Schrock, R. R.; Brookhart, M.; Goldman, A. S. *ACS Catal.* **2013**, *3*, 2505−2514.

(8) Haibach, M. C.; Kundu, S.; Brookhart, M.; Goldman, A. S. *Acc. Chem. Res.* **2012**, *45*, 947−958.

(9) Ahuja, R.; Punji, B.; Findlater, M.; Supplee, C.; Schinski, W.; Brookhart, M.; Goldman, A. S. *Nat. Chem.* **2011**, *3*, 167−171.

(10) (a) Crabtree, R. H.; Mihelcic, J. M.; Quirk, J. M. *J. Am. Chem. Soc.* **1979**, *101*, 7738−7739. (b) Burk, M. J.; Crabtree, R. H. *J. Am. Chem. Soc.* **1987**, *109*, 8025−32. (c) Maguire, J. A.; Boese, W. T.; Goldman, A. S. *J. Am. Chem. Soc.* **1989**, *111*, 7088−7093. (d) Maguire, J. A.; Petrillo, A.; Goldman, A. S. *J. Am. Chem. Soc.* **1992**, *114*, 9492−9498.

(11) Gupta, M.; Hagen, C.; Flesher, R. J.; Kaska, W. C.; Jensen, C. M. *Chem. Commun.* **1996**, 2083−2084.

(12) Liu, F.; Goldman, A. S. *Chem. Commun.* **1999**, 655−656.

(13) Haenel, M. W.; Oevers, S.; Angermund, K.; Kaska, W. C.; Fan, H.-J.; Hall, M. B. *Angew. Chem., Int. Ed.* **2001**, *40*, 3596−3600.

(14) Göttker-Schnetmann, I.; White, P.; Brookhart, M. *J. Am. Chem. Soc.* **2004**, *126*, 1804−1811.

(15) Kuklin, S. A.; Sheloumov, A. M.; Dolgushin, F. M.; Ezernitskaya, M. G.; Peregudov, A. S.; Petrovskii, P. V.; Koridze, A. A. *Organometallics* **2006**, *25*, 5466−5476.

(16) Kundu, S.; Choliy, Y.; Zhuo, G.; Ahuja, R.; Emge, T. J.; Warmuth, R.; Brookhart, M.; Krogh-Jespersen, K.; Goldman, A. S. *Organometallics* **2009**, *28*, 5432−5444.
(17) Punji, B.; Emge, T. J.; Goldman, A. S. *Organometallics* **2010**, *29*, 2702−2709.
(18) Morales-Morales, D.; Redon, R.; Yung, C.; Jensen, C. M. *Inorg. Chim. Acta* **2004**, *357*, 2953−2956.
(19) Göttker-Schnetmann, I.; Brookhart, M. *J. Am. Chem. Soc.* **2004**, *126*, 9330−9338.
(20) Krogh-Jespersen, K.; Czerw, M.; Kanzelberger, M.; Goldman, A. S. *J. Chem. Inf. Comput. Sci.* **2001**, *41*, 56−63.
(21) Krogh-Jespersen, K.; Czerw, M.; Summa, N.; Renkema, K. B.; Achord, P. D.; Goldman, A. S. *J. Am. Chem. Soc.* **2002**, *124*, 11404−11416.
(22) Renkema, K. B.; Kissin, Y. V.; Goldman, A. S. *J. Am. Chem. Soc.* **2003**, *125*, 7770−7771.
(23) Göttker-Schnetmann, I.; White, P. S.; Brookhart, M. *Organometallics* **2004**, *23*, 1766−1776.
(24) Goettker-Schnetmann, I.; Heinekey, D. M.; Brookhart, M. *J. Am. Chem. Soc.* **2006**, *128*, 17114−17119.
(25) (a) Malcolmson, S. J.; Meek, S. J.; Sattely, E. S.; Schrock, R. R.; Hoveyda, A. H. *Nature* **2008**, *456*, 933−937. (b) Ibrahem, I.; Yu, M.; Schrock, R. R.; Hoveyda, A. H. *J. Am. Chem. Soc.* **2009**, *131*, 3844−3845. (c) Flook, M. M.; Jiang, A. J.; Schrock, R. R.; Muller, P.; Hoveyda, A. H. *J. Am. Chem. Soc.* **2009**, *131*, 7962−7963.
(26) (a) Wang, D. Y.; Choliy, Y.; Krogh-Jespersen, K.; Hartwig, J. F.; Goldman, A. S. Abstracts of Papers. In Proceedings of the 240th ACS National Meeting, Boston, MA, August 22−26, 2010; ACS: Washington, DC, 2010, INOR-5. (b) Wang, D. Y.; Krogh-Jespersen, K.; Goldman, A. S. Abstracts of Papers. In Proceedings of the 244th ACS National Meeting and Exposition, Philadelphia, PA, August 19−23, 2012; ACS: Washington, DC, 2012, INOR-587. (c) Wang, D. Y. Ph. D. Thesis, Rutgers University: New Brunswick, NJ, 2012. The origin of this effect will be discussed in detail in a forthcoming publication.
(27) (a) Ozerov, O. V.; Guo, C.; Papkov, V. A.; Foxman, B. M. *J. Am. Chem. Soc.* **2004**, *126*, 4792−4793. (b) Weng, W.; Guo, C.; Moura, C.; Yang, L.; Foxman, B. M.; Ozerov, O. V. *Organometallics* **2005**, *24*, 3487−3499. (c) Gatard, S.; Celenligil-Cetin, R.; Guo, C.; Foxman, B. M.; Ozerov, O. V. *J. Am. Chem. Soc.* **2006**, *128*, 2808−2809. (d) Weng, W.; Guo, C.; Celenligil-Cetin, R.; Foxman, B. M.; Ozerov, O. V. *Chem. Commun.* **2006**, 197−199.
(28) The pK_a values are in DMSO. Source: http://www.chem.wisc.edu/areas/reich/pkatable/index.htm.
(29) Britovsek, G. J. P.; Gibson, V. C.; Hoarau, O. D.; Spitzmesser, S. K.; White, A. J. P.; Williams, D. J. *Inorg. Chem.* **2003**, *42*, 3454−3465.
(30) Lee, D. W.; Kaska, W. C.; Jensen, C. M. *Organometallics* **1998**, *17*, 1−3.
(31) While the stable isomer of (^{carb}PNP)IrH_2(C_2H_4) is the *cis*-isomer, **3c**, treatment of (^{tBu}PCP)IrH_2 with ethylene at −90 °C results in formation of the *trans*-dihydride (^{tBu}PCP)IrH_2(C_2H_4). The increased stability of the *cis*-dihydride in the case of the carbazole system is likely in part due to the decreased *trans* effect of the carbazide nitrogen in **3a** relative to the sp^2 carbon the (PCP)Ir complex thereby favoring the *cis*-dihydride structure which places hydride *trans* to nitrogen, although the greater steric demand of *t*-Bu vs *i*-Pr groups likely also plays an important role. Other iridium ethylene dihydride complexes of which we are aware are the facially substituted cationic $L_3IrH_2(C_2H_4)^+$ where the hydrides are forced to be *cis*. See: (a) Barbaro, P.; Bianchini, C.; Meli, A.; Peruzzini, M.; Vacca, A.; Vizza, F. *Organometallics* **1991**, *10*, 2227−2238. (b) Garcia-Camprubi, A.; Martin, M.; Sola, E. *Inorg. Chem.* **2010**, *49*, 10649−10657.
(32) Peverati, R.; Truhlar, D. G. *J. Phys. Chem. Lett.* **2011**, *2*, 2810−2817.
(33) Biswas, S.; Zhou, T.; Wang, D. Y.; Hackenberg, J.; Nawara-Hultzsch, A.; Schrock, R. R.; Brookhart, M.; Krogh-Jespersen, K.; Goldman, A. S. Abstracts of Papers. In Proceedings of the 245th ACS National Meeting and Exposition, New Orleans, LA, April 7−11, 2013; ACS: Washington, DC, 2013, INOR-681. The origin of the kinetic barrier will be discussed in detail in a forthcoming publication.
(34) Jean, Y.; Eisenstein, O. *Polyhedron* **1988**, *7*, 405−407.
(35) Riehl, J. F.; Jean, Y.; Eisenstein, O.; Pelissier, M. *Organometallics* **1992**, *11*, 729−737.
(36) The van der Waals radii of Ir and H are reported as 202 and 110 pm, respectively. http://periodic.lanl.gov/index.shtml.
(37) (a) Brookhart, M.; Green, M. L. H. *J. Organomet. Chem.* **1983**, *250*, 395−408. (b) Brookhart, M.; Green, M. L. H.; Parkin, G. *Proc. Natl. Acad. Sci. U. S. A.* **2007**, *104*, 6908−6914.
(38) The present authors are not qualified to comment with authority on the probable causes for this significant disagreement among the functionals. We note, however, that M11 is a range-separated hybrid functional containing a contribution of 42.8% Hartree−Fock (HF) exchange to the short-range interelectronic interactions but 100% HF exchange to the long-range interactions, whereas M11-L is a local functional with a dual-range local exchange functional (i.e., 0% HF exchange). M06-L is also a local functional, whereas M06 is a hybrid functional with 27% HF exchange; neither M06-L nor M06 features range-separation. It is tempting to associate the exceedingly large barrier produced by the M11 functionals, relative to the barriers predicted by M11-L, M06-L, and M06 functionals and experiment, with differences in the treatment of electron exchange and, in particular, the large admixture of HF exchange present in M11.
(39) See, e.g. Bersuker, I. B. The Jahn-Teller Effect: Implications in Electronic Structure Calculations. In *Progress in Theoretical Chemistry and Physics*; Piecuch, P., Maruani, J., Delgado-Barrio, G., Wilson, S., Eds.; Springer: New York, 2009; Vol. *19*; pp 343−362.
(40) The barrier predicted by M11-L (23.6 kcal/mol) is in fact very close to the experimental value (21 kcal/mol). We note that M11-L is intended to '... provide broad accuracy for both single-configurational and multiconfigurational molecules and for solid-state lattice constants.' Peverati, R.; Truhlar, D. C. *J. Phys. Chem. Lett.* **2012**, *3*, 117−124.
(41) (a) Wick, D. D.; Goldberg, K. I. *J. Am. Chem. Soc.* **1997**, *119*, 10235−10236. (b) Bartlett, K. L.; Goldberg, K. I.; Borden, W. T. *J. Am. Chem. Soc.* **2000**, *122*, 1456−1465. (c) Bartlett, K. L.; Goldberg, K. I.; Borden, W. T. *Organometallics* **2001**, *20*, 2669−2678. (d) Fekl, U.; Goldberg, K. I. *J. Am. Chem. Soc.* **2002**, *124*, 6804−6805.
(42) Elliot, A. J.; McCracken, D. R.; Buxton, G. V.; Wood, N. D. *J. Chem. Soc. Faraday Trans.* **1990**, *86*, 1539−1547.
(43) Perutz, R. N.; Sabo-Etienne, S. *Angew. Chem., Int. Ed.* **2007**, *46*, 2578−2592.
(44) Campos, J.; Kundu, S.; Pahls, D. R.; Brookhart, M.; Carmona, E.; Cundari, T. R. *J. Am. Chem. Soc.* **2013**, *135*, 1217−1220.
(45) Saillard, J.; Hoffmann, R. *J. Am. Chem. Soc.* **1984**, *106*, 2006−2026.
(46) Lundquist, E. G.; Huffman, J. C.; Folting, K.; Caulton, K. G. *Angew. Chem., Int. Ed. Engl.* **1988**, *27*, 1165−1167.
(47) Crabtree, R. *Acc. Chem. Res.* **1979**, *12*, 331−337.
(48) Brandt, P.; Hedberg, C.; Andersson, P. G. *Chem. - Eur. J.* **2003**, *9*, 339−347.
(49) Helmchen, G. n.; Pfaltz, A. *Acc. Chem. Res.* **2000**, *33*, 336−345.
(50) Cui, X.; Fan, Y.; Hall, M. B.; Burgess, K. *Chem. - Eur. J.* **2005**, *11*, 6859−6868.
(51) Bianchini, C.; Farnetti, E.; Graziani, M.; Kaspar, J.; Vizza, F. *J. Am. Chem. Soc.* **1993**, *115*, 1753−1759. The authors note that other mechanistic interpretations are possible.
(52) Onderdelinden, A. L.; van der Ent, A. *Inorg. Chim. Acta* **1972**, 420−426.
(53) Andrae, D.; Haeussermann, U.; Dolg, M.; Stoll, H.; Preuss, H. *Theor. Chim. Acta* **1990**, *77*, 123−41.
(54) (a) Krishnan, R.; Binkley, J. S.; Seeger, R.; Pople, J. A. *J. Chem. Phys.* **1980**, *72*, 650. (b) McLean, A. D.; Chandler, G. S. *J. Chem. Phys.* **1980**, *72*, 5639.